J. Fluid Mech. (2026), *vol.* 1029, A55, doi:10.1017/jfm.2026.11237

JFM PAPERS

An interaction mechanism sustaining near-equilibrium shielded geophysical vortices

Victoria Christine Zoeller[1], **Jean Noel Reinaud**[2], **Álvaro Viúdez**[1] and **David Gerard Dritschel**[2]

[1]Departament d'Oceanografia Física i Technològica, Institut de Ciències del Mar (ICM), CSIC, Barcelona 08003, Spain

[2]School of Mathematics and Statistics, University of St Andrews, North Haugh, St Andrews KY16 9SS, UK

Corresponding author: Álvaro Viúdez, aviudez@cmima.csic.es

(Received 14 February 2025; revised 6 November 2025; accepted 26 January 2026)

We investigate the interaction between two equally signed neutral vortices, namely vortices with a vanishing area integral of vorticity in inviscid non–divergent two-dimensional flows or a vanishing volume integral of potential vorticity anomaly in three-dimensional quasi-geostrophic (QG) flows. The vortices have a continuous (potential) vorticity distribution, and are linear combinations of appropriately normalised cylindrical (or spherical) Bessel functions of order 0, truncated at a zero of the Bessel function of order 1. Some pairs of neutral vortices reach an oscillating near-equilibrium state, attracting and repelling each other as a result of the exchange of small amounts of vorticity in their peripheries. This vorticity exchange generates a dipolar moment within each vortex which separates the vortices slightly, whereas the subsequent radial redistribution of the vorticity causes the vortices to come back closer again. The interaction is slower and weaker in three-dimensional QG flows, as the potential vorticity exchange primarily takes place close to the horizontal mid-plane of the vortices. These results have been corroborated using two radically different numerical models, namely a pseudo-spectral model and a high-resolution contour-advection model, both in two and in three dimensions. The observed oscillation mechanism could explain the persistence of geophysical vortices under the influence of other vortices and their ability to form stable vortex structures without experiencing vortex merging.

Key words: quasi-geostrophic flows, vortex dynamics, vortex interactions

1. Introduction

Mesoscale and submesoscale ocean vortices play an important role in the distribution of heat, salt and other tracers in the global ocean circulation. These vortices proliferate in both the oceans and atmosphere, and they frequently interact with currents and other vortices (Yasuda, Okuda & Hirai 1992; Schultz Tokos, Hinrichsen & Zenk 1994; Paireau, Tabeling & Legras 1997; Carton *et al.* 2010; Rodríguez-Marroyo *et al.* 2011; Chouksey 2023; Zoeller & Viúdez 2024). In the Mediterranean Sea, for example, Carton *et al.* (2010) compared experimental observations with the results of a three-layer quasi-geostrophic numerical model and concluded that mesoscale vortices interact via their mutual advection by partner vortices. Arguably, understanding the dynamics of mesoscale and submesoscale vortices, and in particular their interactions, is essential to understanding the dynamics of the whole ocean.

Early experimental studies of Brown & Roshko (1974) and Winant & Browand (1974) showed that, in a turbulent mixing layer, like-sign vortices can merge, thereby forming a larger vortex. Vortices may merge if the distance separating them is less than a threshold known as the critical merger distance, see Dritschel (1995), Reinaud & Dritschel (2005) and references therein. Vortex merger, also known as coalescence or fusion, has been exhaustively described in many experimental and numerical studies (Christiansen & Zabusky 1973; Dritschel 1985; Melander, Zabusky & Mcwilliams 1988; Dritschel & Waugh 1992; Waugh 1992; Ritchie & Holland 1993; Perrot & Carton 2010; Ciani, Carton & Verron 2016). The merger of shielded vortices, i.e. vortices consisting of a core surrounded by an opposite-signed vorticity annulus may, however, be inhibited when the vorticity distributions are not overlapping (Ritchie & Holland 1993; Valcke & Verron 1997; Carton 2001). In this respect Carton (1992) concluded that shielding generally reduces the critical separation distance for merging, and moreover, in some cases, barotropic instability within each vortex may inhibit their merging. Indeed, in some shielded vortices, the vorticity of the annulus re-organises to generate dipolar moments which make the vortices move apart before they can merge.

The interaction of two shielded vortices depends on their initial separation, their vorticity distribution and other properties such as the baroclinicity and stratification (Carton 1992; Chan & Law 1995; Valcke & Verron 1997). In particular, it has been observed that ocean vortices remain approximately isolated and present a shield of relative vorticity, that is, vertical vorticity relative to the Earth's rotating reference frame (Valcke & Verron 1997; Schmidt *et al.* 1998; Beckers *et al.* 2001; Viúdez 2021; Chouksey 2023). The investigation of how such ocean vortices interact is therefore merited.

It is well known that vortices may either completely merge, partially merge or separate (Ritchie & Holland 1993; Holland & Dietachmayer 1993; Wang & Holland 1995; Valcke & Verron 1997; Ciani *et al.* 2016), but the detailed physical processes responsible for the formation of robust near-equilibrium multipolar structures are still largely unknown. This study focuses on the interaction of two like-signed, continuous, shielded neutral vortices, both in two-dimensional (2-D) and in three-dimensional (3-D) quasi-geostrophic (QG) flows relevant to the atmosphere/ocean dynamics. We find that vortices can reach an oscillating near-equilibrium state where the vortices attract and repel each other through the exchange of peripheral vorticity. We verify that this new form of interaction is a robust process using simulations conducted by two very different numerical methods, namely a pseudo-spectral code and a contour-advection code, both in 2-D and in 3-D QG flows.

This study is structured as follows. Section 2 describes the mathematical and numerical formulation, and explains the initial conditions used, both in 2-D as well as in 3-D QG. Next, the results of our numerical simulations are presented in § 3. Finally, conclusions are offered in § 4.

2. Mathematical and numerical formulation

2.1. *Basic equations*

In the 3-D QG model, the dynamical equation describing the flow evolution under inviscid adiabatic conditions is the material conservation of potential vorticity anomaly (hereafter PVA), denoted by $\varpi^q(\boldsymbol{x}, t)$, where the superscript q indicates quasi-geostrophic dynamics. The PVA is advected by the horizontal geostrophic flow

$$\frac{\partial \varpi^q}{\partial t} + \boldsymbol{u}_h^g \boldsymbol{\cdot} \boldsymbol{\nabla}_h \varpi^q = 0. \tag{2.1}$$

Here, $\boldsymbol{u}_h^g(\boldsymbol{x}, t)$ is the horizontal geostrophic velocity, where h indicates horizontal components and g indicates geostrophic balance, scaled by f_0^{-1}, where f_0 is the constant background planetary vorticity, or Coriolis frequency. The geostrophic velocity $\boldsymbol{u}_h^g$ is defined from the geopotential anomaly field $\phi(\boldsymbol{x}, t)$ by

$$\boldsymbol{u}_h^g \equiv -\boldsymbol{\nabla} \times (\phi\, \hat{\boldsymbol{z}}). \tag{2.2}$$

The QG PVA,

$$\varpi^q \equiv \zeta^g + \mathcal{S} = \hat{\nabla}^2 \phi, \tag{2.3}$$

is defined as the sum of the vertical component of geostrophic vorticity $\zeta^g(\boldsymbol{x}, t)$ and the dimensionless vertical stratification anomaly $\mathcal{S}(\boldsymbol{x}, t)$. The operator $\hat{\boldsymbol{\nabla}}$ is the 3-D gradient in the rescaled coordinates $(x, y, \hat{z})$. Under the leading-order geostrophic approximation, the vertical vorticity

$$\zeta^g \equiv \hat{\boldsymbol{z}} \boldsymbol{\cdot} \boldsymbol{\nabla} \times \boldsymbol{u}_h^g, \tag{2.4}$$

becomes the horizontal Laplacian of the geopotential

$$\zeta^g = \nabla_h^2 \phi. \tag{2.5}$$

The dimensionless vertical stratification anomaly takes the form

$$\mathcal{S} \equiv -\frac{\partial D}{\partial z} = \frac{\partial^2 \phi}{\partial \hat{z}^2}, \tag{2.6}$$

where $D(\boldsymbol{x}, t)$ is the vertical isopycnal displacement, while $\hat{z} \equiv (N_0/f_0)z$ is the stretched QG vertical coordinate, with N_0 being a constant background Brunt–Väisälä frequency. The vertical isopycnal displacement $D(\boldsymbol{x}, t) \equiv z - \eta(\boldsymbol{x}, t)$, where $\eta(\boldsymbol{x}, t)$ is the vertical location that an isopycnal located at $\boldsymbol{x}$ at time t has in the reference configuration defined by $\varrho_Z z + \rho_0$. The density anomaly is $\rho'(\boldsymbol{x}, t) \equiv \rho(\boldsymbol{x}, t) - \varrho_Z z - \rho_0$, where $\rho(\boldsymbol{x}, t)$ is the mass density, and ρ_0 and ϱ_Z are a constant background density and a constant background density stratification. Thus, the density field is expressed in terms of displacements.

In the 2-D model of non–divergent Euler flows, the governing equation reduces to the material conservation of vertical vorticity $\zeta(\boldsymbol{x}_h, t)$

$$\frac{\mathrm{d}\zeta}{\mathrm{d}t} \equiv \frac{\partial \zeta}{\partial t} + \boldsymbol{u}_h \boldsymbol{\cdot} \boldsymbol{\nabla}_h \zeta = 0, \tag{2.7}$$

where $\boldsymbol{u}_h(\boldsymbol{x}_h, t)$ is the divergence-free horizontal velocity and $\boldsymbol{\nabla}_h$ is the 2-D gradient operator.

2.2. *Initial conditions*

This subsection describes the initial conditions used in the 2-D and 3-D QG numerical simulations.

2.2.1. *Two-dimensional flows*

Following Viúdez (2021), the initial vorticity field consists of a finite linear combination of shifted, normalised and truncated cylindrical Bessel modes of order 0, $J_0(\kappa\rho)$, where κ is the cylindrical radial wavenumber ($\kappa = 1$ in the results below), and ρ is the cylindrical radius of the polar coordinate system (ρ, φ). The Bessel modes are truncated at the pth zero of the cylindrical Bessel function of order 1, namely $j_{1,p}$, where $p \in \mathbb{N}$, arranged so that $J_1(j_{1,p}) = 0$. Each vorticity layer mode, $\zeta_p(\rho)$, is defined piecewise as

$$\zeta_p(\rho) \equiv 2c_p \begin{cases} J_0(\kappa\rho) - J_0(j_{1,p}) & \kappa\rho \le j_{1,p} \\ 0 & \kappa\rho > j_{1,p}, \end{cases} \tag{2.8}$$

where c_p is a normalisation constant defined by

$$c_p \equiv -\frac{\kappa^2}{J_0(j_{1,p})\, j_{1,p}^2}. \tag{2.9}$$

The value of c_p ensures that each layer-mode ζ_p has the same area integral of vorticity (circulation), without loss of generality taken to be 2π

$$\int_0^{2\pi} \int_0^{j_{1,p}/\kappa} \zeta_p(\rho)\, \rho\, \mathrm{d}\rho\, \mathrm{d}\varphi = 2\pi. \tag{2.10}$$

A vortex is thus constructed as a linear superposition of N layer modes

$$\zeta_{a_1,a_2,\ldots a_N}(\rho) \equiv \sum_{p=1}^{N} a_p \zeta_p(\rho), \tag{2.11}$$

where a_p is the amplitude of mode p. Since each layer-mode ζ_p has the same area integral of vorticity, neutral vortices satisfy the relation

$$\sum_{p=1}^{N} a_p = 0. \tag{2.12}$$

2.2.2. *Three-dimensional QG flows*

In the 3-D QG model, the initial PVA field consists of a finite superposition of radial PVA layer modes $\varpi_p(r)$ (see Zoeller & Viúdez 2023*b*). The layer modes are spherically symmetric, with a PVA distribution given by a truncated, shifted and normalised spherical Bessel mode of order 0, $j_0(kr)$, where k is the spherical radial wavenumber ($k = 1$ in the results below). Its boundary radius coincides with a zero $j_{3/2,p}$ of the first-order spherical Bessel function $j_1(kr)$, so that $j_1(j_{3/2,p}) = 0$. Each PVA layer-mode $\varpi_p(r)$ is defined piecewise as

$$\varpi_p(r) \equiv 2C_p k^3 \begin{cases} j_0\left(j_{3/2,p}\right) - j_0\left(kr\right) & kr \le j_{3/2,p} \\ 0 & kr > j_{3/2,p}, \end{cases} \tag{2.13}$$

where C_p is a normalisation constant given by

$$C_p \equiv \frac{3}{4 j_0\left(j_{3/2,p}\right)\, j_{3/2,p}^3}. \tag{2.14}$$

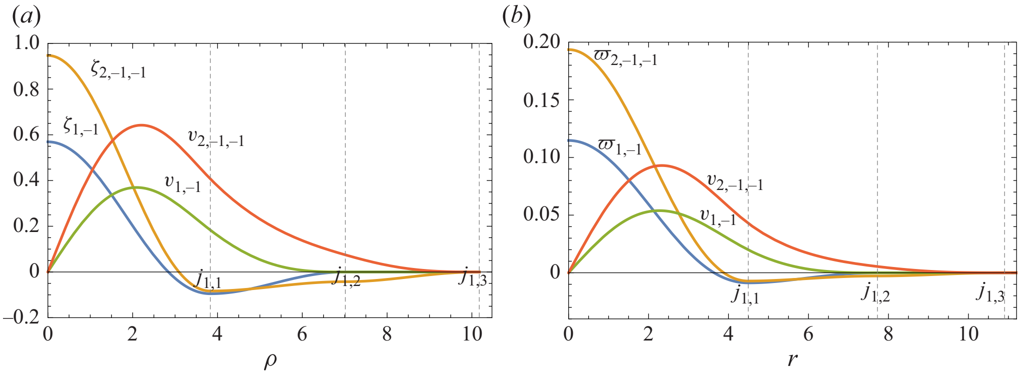

Figure 1. Vorticity (ζ, ϖ) and azimuthal velocity (v) profiles for both (*a*) 2-D and (*b*) 3-D QG vortices.

This constant is chosen so that each layer mode for $p = 1, 2, \ldots$ has the same volume integral of PVA, namely

$$\int_0^{2\pi} \int_0^{\pi} \int_0^{j_{3/2,p}/k} \varpi_p(r)\, r^2 \sin\theta \,\mathrm{d}r\, \mathrm{d}\theta\, \mathrm{d}\varphi = 2\pi, \tag{2.15}$$

in spherical coordinates (r, θ, φ).

As in the 2-D case, we define the initial PVA distribution $\varpi(r)$ as a superposition of N PVA layer modes

$$\varpi(r) \equiv \sum_{p=1}^{N} a_p \varpi_p(r). \tag{2.16}$$

In the case of neutral vortices, defined as vortices having a vanishing volume integral of PVA, the sum of the layer-mode coefficients a_p vanishes

$$\sum_p^N a_p = 0. \tag{2.17}$$

Although in general $a_p \in \mathbb{R}$, we restrict these values to $a_p \in \mathbb{Z}$. Thus, every vortex may be defined by its initial PVA configuration, given by an N-tuple of layer-mode coefficients $\boldsymbol{a} \equiv \{a_1, \ldots, a_N\}$.

In this study we use two of the simplest neutral vortices one may construct in either the 2-D or 3-D QG cases. The first is a two-layer vortex, which is known to evolve spontaneously into a stable tripolar structure (Viúdez 2021; Zoeller & Viúdez 2023*b*), and has vorticity and PVA distributions

$$\zeta_{1,-1}(\rho) \equiv \zeta_1(\rho) - \zeta_2(\rho) \quad \text{and} \quad \varpi_{1,-1}(r) \equiv \varpi_1(r) - \varpi_2(r). \tag{2.18a,b}$$

The second vortex is a stable, axisymmetric three-layer vortex with vorticity and PVA distributions given by

$$\zeta_{2,-1,-1}(\rho) \equiv 2\zeta_1(\rho) - \zeta_2(\rho) - \zeta_3(\rho) \quad \text{and} \quad \varpi_{2,-1,-1}(r) \equiv 2\varpi_1(r) - \varpi_2(r) - \varpi_3(r). \tag{2.19a,b}$$

For simplicity, we refer to these initial vortex profiles as ζ_u or ϖ_u for the unstable two-layer vortex, and ζ_s or ϖ_s for the stable three-layer vortex. The initial velocity and vorticity profiles for the 2-D and 3-D QG cases are illustrated in figure 1.

https://doi.org/10.1017/jfm.2026.11237 Published online by Cambridge University Press

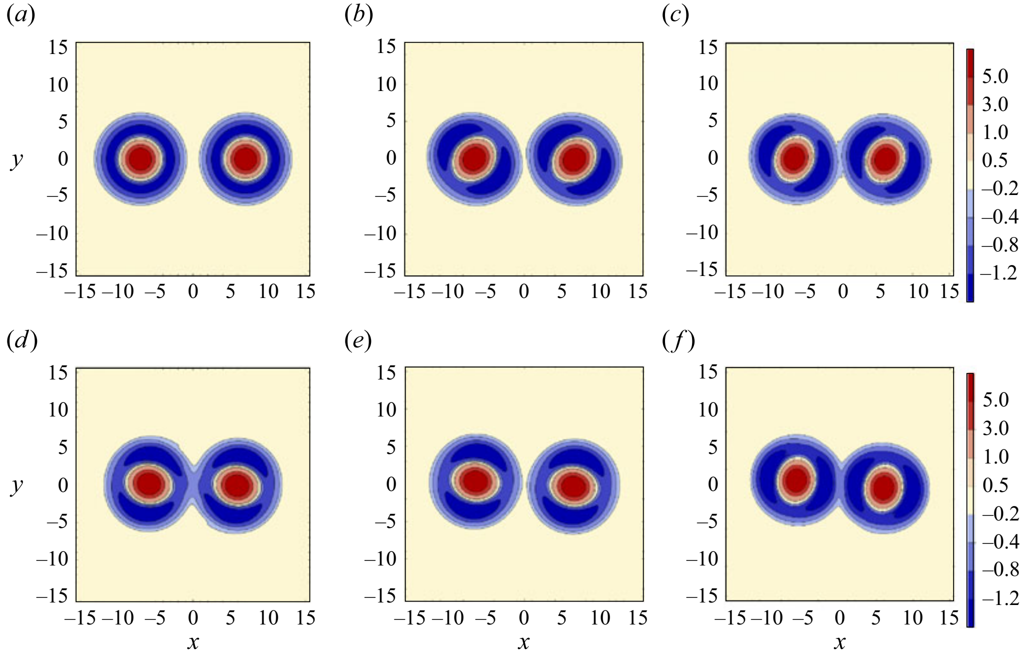

Figure 2. Vorticity field $\zeta \times 10$ of two initially touching ζ_u vortices at times (*a*) $t = 0$, (*b*) $t = 2190$, (*c*) $t = 2580$, (*d*) $t = 3000$, (*e*) $t = 4610$ and (*f*) $t = 5650$, using the 2-D pseudo-spectral code.

2.3. *Numerical algorithms*

We use two different numerical methods to run our simulations and to ensure our main conclusions are robust and do not depend on details of the numerical method. The first one, a purely Eulerian pseudo-spectral method, is detailed in Appendix A. The second one, a hybrid Lagrangian/Eulerian contour-advection method, is detailed in Appendix B. The latter method allows for a particularly fine resolution of the vorticity/potential vorticity field, thereby achieving high accuracy at low computational cost.

3. Numerical results

3.1. *Two-dimensional flows*

This section considers the interaction between two neutral vortices, either with the same initial profile, ζ_u, or with different initial profiles, ζ_s and ζ_u. We investigate the interaction between the vortices for various vortex separations, from touching vortices to vortices separated by $\delta_0 = j_{1,2}$.

3.1.1. *Interaction between ζ_u vortices*

It is known that an isolated (neutral) vortex may destabilise and evolve into a tripole, mainly due to the growth of azimuthal mode $m = 2$ (Carton & Legras 1994; Morel & Carton 1994; Kizner & Khvoles 2004; Trieling *et al.* 2010; Viúdez 2021). The time evolution of two ζ_u vortices whose boundaries are touching initially is shown in figure 2. At the initial time, when the two neutral vortices are placed close together (but not overlapping), the vortices do not interact, as the flow field due to each vortex vanishes beyond their boundary. Afterwards, as expected, an azimuthal mode 2 develops on the vortices from numerical noise, eventually causing them to reorganise into robust (stable)

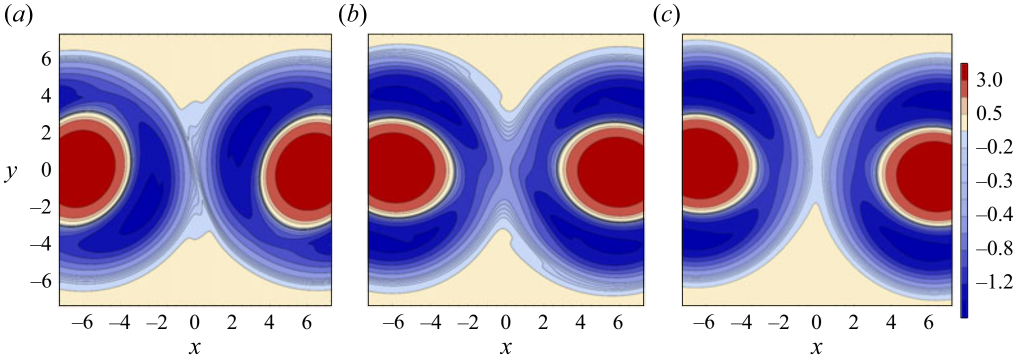

Figure 3. Zoom of the interaction shown in figure 2 (*c*), (*d*), (*e*) of the vorticity $\zeta \times 10$ at times (*a*) $t = 2580$, (*b*) $t = 3000$, (*c*) $t = 4610$.

tripoles. These tripolar structures now produce an external potential flow (absent for the original vortices). This causes small anomalies in the negative vorticity poles which are no longer perfectly aligned with the positive centre of the vortex core, causing the vortices to move, specifically to attract and eventually exchange vorticity at two different locations symmetrically (figure 3). When in contact, the vortices touch along a curve. Vorticity is then exchanged across the contact curve, redistributing negative vorticity between the two vortices. This exchange generates a dipolar moment within each vortex which (by advection) transfers negative vorticity from one vortex to the other. In this sense, the left vortex transfers negative vorticity at a location $y < 0$ to the right vortex, but amplifies negative vorticity at a location $y > 0$ (figure 3). This slightly changed vorticity anomaly distribution, or dipolar moment, causes each vortex to move in the opposite direction, so that the vortices repel slightly. These vorticity changes are, however, rapidly redistributed azimuthally along the vortex periphery so that their dipolar moment weakens, and the vortices start approaching again figure 2. In this manner, the tripolar structures reach an oscillating near-equilibrium state, where vorticity exchange and vorticity redistribution take place nearly periodically.

The pseudo-spectral and the contour-advection simulations produce similar qualitative results, as shown in figures 2 and 4. In both simulations the ζ_u vortex evolves into a stable tripole and both capture the vortex interaction arising from vorticity exchange, and an alternating attraction and repulsion between the vortices.

This mechanism of vorticity exchange leading to an oscillating near-equilibrium state is new. It has already been shown that two shielded vortices that are in close proximity may evolve through different near-equilibrium states, attracting and/or repelling each other, depending on the changes in the vorticity distribution of their outer shield (Carton 1992; Holland & Dietachmayer 1993; Valcke & Verron 1997; Carton *et al.* 2016). However, in most cases, excepting very weak interactions, the interaction results in either the formation of a larger merged vortex, a partial merger or straining out where smaller vortices are formed or the repulsion of the two vortices (Carton 1992; Ritchie & Holland 1993; Holland & Dietachmayer 1993; Chan & Law 1995; Dritschel 1995; Wang & Holland 1995; Valcke & Verron 1997; Reinaud & Dritschel 2005).

The observed differences between the pseudo-spectral and contour-advection simulations mainly concern the precise location of the vortices and the time it takes for the vortices to interact. Such differences are expected because of the very long integration times required for these interaction processes to develop, and the accumulated impact of hyperviscosity in the pseudo-spectral model. As a result, the vorticity leakage in the

https://doi.org/10.1017/jfm.2026.11237 Published online by Cambridge University Press

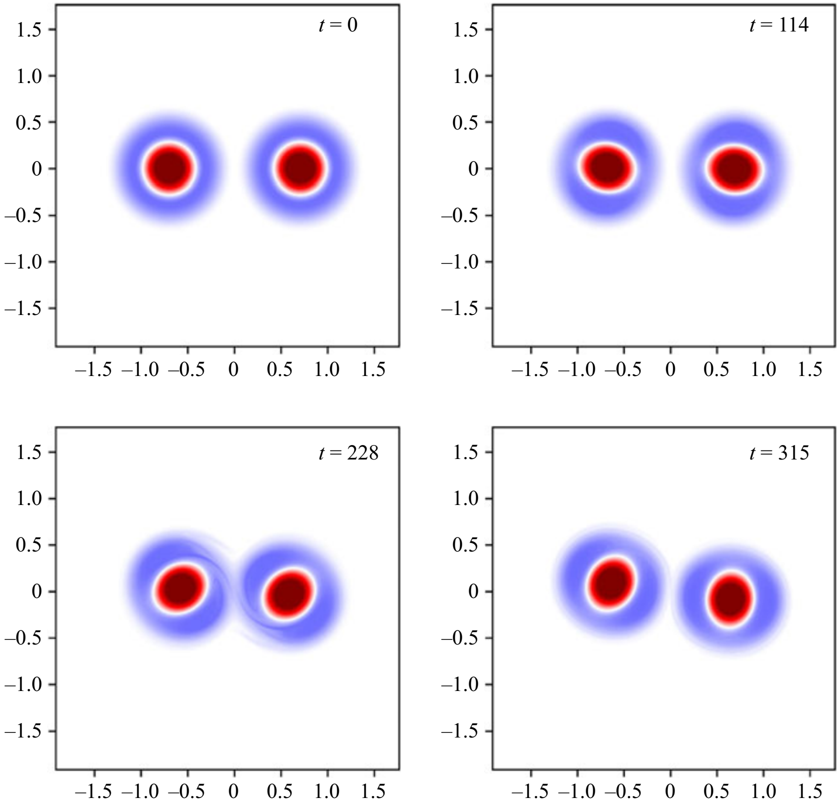

Figure 4. Evolution of the vorticity $\zeta \times 10$ of two initially touching ζ_u vortices, here using the 2-D contour-advection code, combined Lagrangian advection method (CLAM).

contour-advection simulation is larger, thus the tripolar structures rotate faster and their displacement is larger than in the pseudo-spectral simulation, cf. Figure 4.

The motion of each vortex has two components, one due to the rotating vorticity poles (anomalies) within the tripole, and the other due to the potential flow generated by its tripole partner. An analysis of the relative motion of the two touching ζ_u vortices for the contour-advection simulation follows. The centre of each vortex $\boldsymbol{X}_j$ (for $j = 1,\ 2$) over the time interval $80 \leq t < 592$ is computed every data-save interval $\Delta t = 1$. The vortex centres are defined as the geometric centre of the two contiguous regions where the vorticity exceeds the root-mean-square value of the vorticity field in the domain. The vorticity field is split into two parts: the inner vorticity field, $q_i^j(\boldsymbol{x}, t)$, and the outer vorticity field, $q_o^j(\boldsymbol{x}, t)$, for $j = 1, 2$. These are defined by

$$q_i^j(\boldsymbol{x}, t) \equiv \begin{cases} q(\boldsymbol{x}, t), & |\boldsymbol{x} - \boldsymbol{X}_j| \leq r_c, \\ 0, & |\boldsymbol{x} - \boldsymbol{X}_j| > r_c \end{cases}, \qquad q_o^j(\boldsymbol{x}, t) \equiv \begin{cases} 0, & |\boldsymbol{x} - \boldsymbol{X}_j| \leq r_c, \\ q(\boldsymbol{x}, t) & |\boldsymbol{x} - \boldsymbol{X}_j| > r_c, \end{cases} \tag{3.1}$$

where $r_c \equiv \alpha R_0$, with R_0 the initial vortex radius. In practice, we set $\alpha = 1.05$ to take into account the deformation of the vortices. We then evaluate the velocities $\boldsymbol{u}_{i,o}^j$ induced by $q_{i,o}^j$ and define $w_{i,o}^j \equiv \boldsymbol{u}_{i,o}^j \boldsymbol{\cdot} \boldsymbol{t}^j$ as the projection of the induced velocity parallel to the line

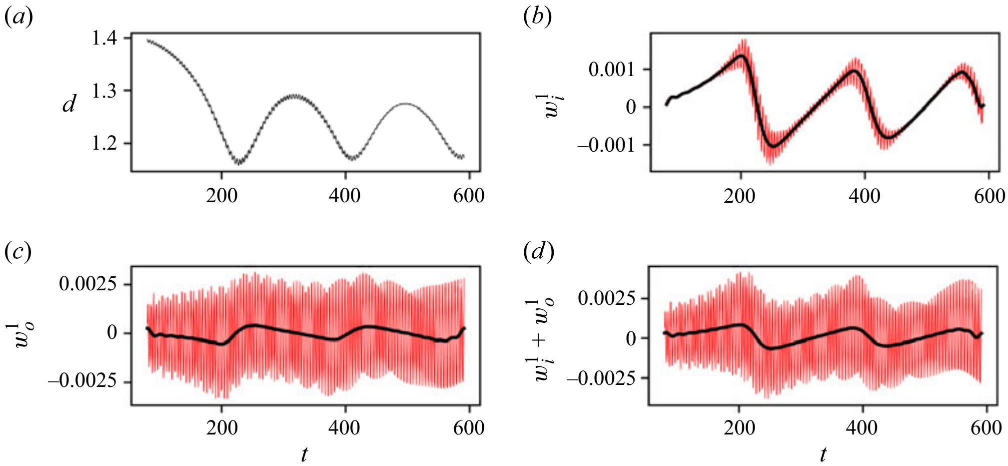

Figure 5. Interaction of two initially touching ζ_u vortices simulated using the 2-D contour-advection model, CLAM. The panels show the evolution of various diagnostics: (*a*) the distance d between the two vortex centres; (*b*) the projected velocity w_i^1 (red) and the low-pass filtered projected velocity $\bar{w}_i^1$ (black); (*c*) the projected velocity w_o^1 (red) and the low-pass filtered projected velocity $\bar{w}_o^1$ (black); (*d*) the full projected velocity $w_i^1 + w_o^1$;.

joining the two vortex centres. Here, $\boldsymbol{t}^j$ is the unit vector in the direction $\boldsymbol{X}_{3-j} - \boldsymbol{X}_j$. Therefore a velocity $w_{i,o}^j > 0$ makes vortex j move towards vortex $3 - j$.

Results for $d = |\boldsymbol{X}_2 - \boldsymbol{X}_1|$ and $w_{i,o}^1$ are presented in figure 5 (results for $w_{i,o}^2$ are virtually identical and are not shown). They show that the distance between the two vortex centres is characterised by fast, small-amplitude oscillations superimposed on a slow evolution. These fast oscillations dominate the evolution of the projected velocity w_o^j but are also noticeable in the evolution of w_i^j. They are caused by the rotation of the tripoles. To extract the slow motion, the fast oscillations were filtered out from $w_{i,o}^j$ by applying a low-pass spectral filter over the time interval $80 \leq t < 592$. To do this, we perform a Fourier transform of $w_{i,o}^j$ and set to zero all Fourier coefficients having wavenumbers exceeding 30; a subsequent inverse transform defines the filtered velocities $\bar{w}_{i,o}^j$. The results show that the full projected velocity $w_i^j + w_o^j$, and hence the overall relative motion, is dominated by the self-induced velocity field w_i^j (figure 5). This velocity is due to the dipolar moment that arises from the misalignment of the vorticity poles relative to the tripole centre (i.e. they are not co-linear), a finding which is consistent with previous studies (Holland & Dietachmayer 1993; Chan & Law 1995).

3.1.2. *Interaction between ζ_s and ζ_u vortices*

The interaction of different neutral vortices, a ζ_u and a ζ_s vortex, is discussed next. We illustrate one case where the vortices are initially separated by a distance $\delta_0 = 0.5 j_{1,2}$ between their boundaries (figure 6). The evolution is qualitatively similar to the evolution described in § 3.1.1. The ζ_u vortex evolves, as expected, into a robust compact tripole, while the ζ_s vortex hardly deforms at all (figure 6*b*). The linear stability analysis for both a ζ_u and a ζ_s vortex when isolated may be found in Appendix C. Only the tripole then generates an exterior potential flow and the vortices attract until they exchange negative vorticity at their peripheries (figure 6*c*). This vorticity exchange again generates a dipolar moment

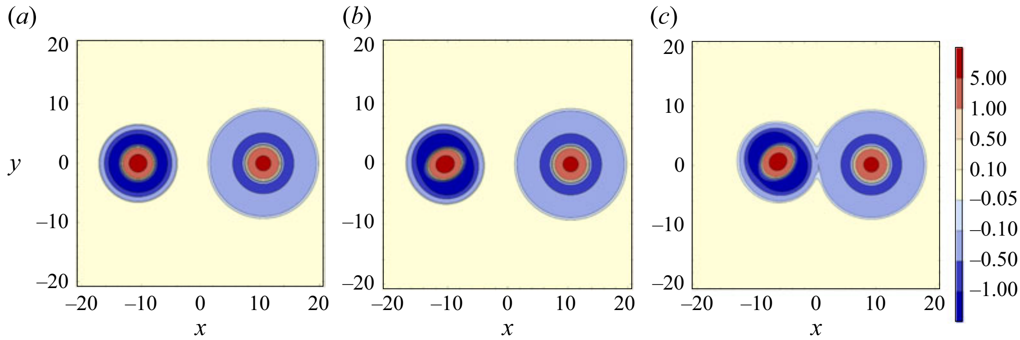

Figure 6. Evolution of the vorticity $\zeta \times 10$ of the ζ_u and ζ_s vortices at times (*a*) $t = 0$, (*b*) $t = 5000$, (*c*) $t = 38\,720$ using the 2-D pseudo-spectral code.

in each vortex, which makes them move apart slightly, until the vorticity anomalies are redistributed along the vortex peripheries and the vortices start approaching again. The two vortices maintain an oscillating, near-equilibrium state due to peripheral vorticity exchange and vorticity redistribution. During this interaction the ζ_s vortex is only very weakly disturbed.

The vortex evolution depends weakly on the initial distance δ_0 between vortices. When the vortex outer layers are initially touching, the near-equilibrium state exhibits oscillations of small amplitude. When δ_0 increases the vortices also evolve towards a near-equilibrium state, exchanging vorticity, alternatively attracting and repelling each other, but the oscillations become less periodic and the separation distance between them oscillates with larger amplitude. In these cases, the rotation rate of the whole vortex structure is larger, which is associated with the greater erosion of negative vorticity into the exterior flow in form of thin vortex filaments.

3.2. *Three-dimensional quasi-geostrophic flows*

As in 2-D flows, isolated (neutral) vortices may destabilise and evolve into tripoles in 3-D QG flows (Zoeller & Viúdez 2023*b*; Barabinot *et al.* 2024). The ϖ_u vortices evolve into spheroidal stable compact tripoles, and therefore generate an exterior potential flow. The re-organisation of the vortices into tripoles is due to the growth of an azimuthal mode with $m = 2$ as found previously for 2-D vortices. However, once the vortices closely approach, higher modes develop similar to those seen in previous surface QG numerical simulations (Carton *et al.* 2016).

Notably, 3-D QG vortices having comparable maximum vorticity approach much more slowly than their 2-D counterparts. This is due to the facts that (i) the turnover period of a 2-D circular patch of uniform vorticity ζ_0 is $T_a = 4\pi/\zeta_0$ while it is $T_a = 6\pi/\varpi_0$ for a 3-D QG spherical vortex of uniform PVA ϖ_0, and (ii) the exterior velocity field decays as $1/r$ in two dimensions, while decays as $1/r^2$ in 3-D QG, where r is the distance from the vortex centre. In fact, it decays even more strongly for neutral vortices having a tripolar shape, by a further factor of r.

The interaction of two ϖ_u vortices is shown in figure 7, both from a vertical and a horizontal perspective (top and bottom rows, respectively). Initially, an $m = 2$ perturbation with amplitude 100 times smaller than the peak PVA is added to speed up the early stages of evolution. The spheroidal shape of the QG vortices makes the interaction between the two vortices weaker, since the exchange of PVA takes place mainly near the mid-plane $z = 0$ where the vortices touch. By contrast, close non-neutral 3-D QG vortices

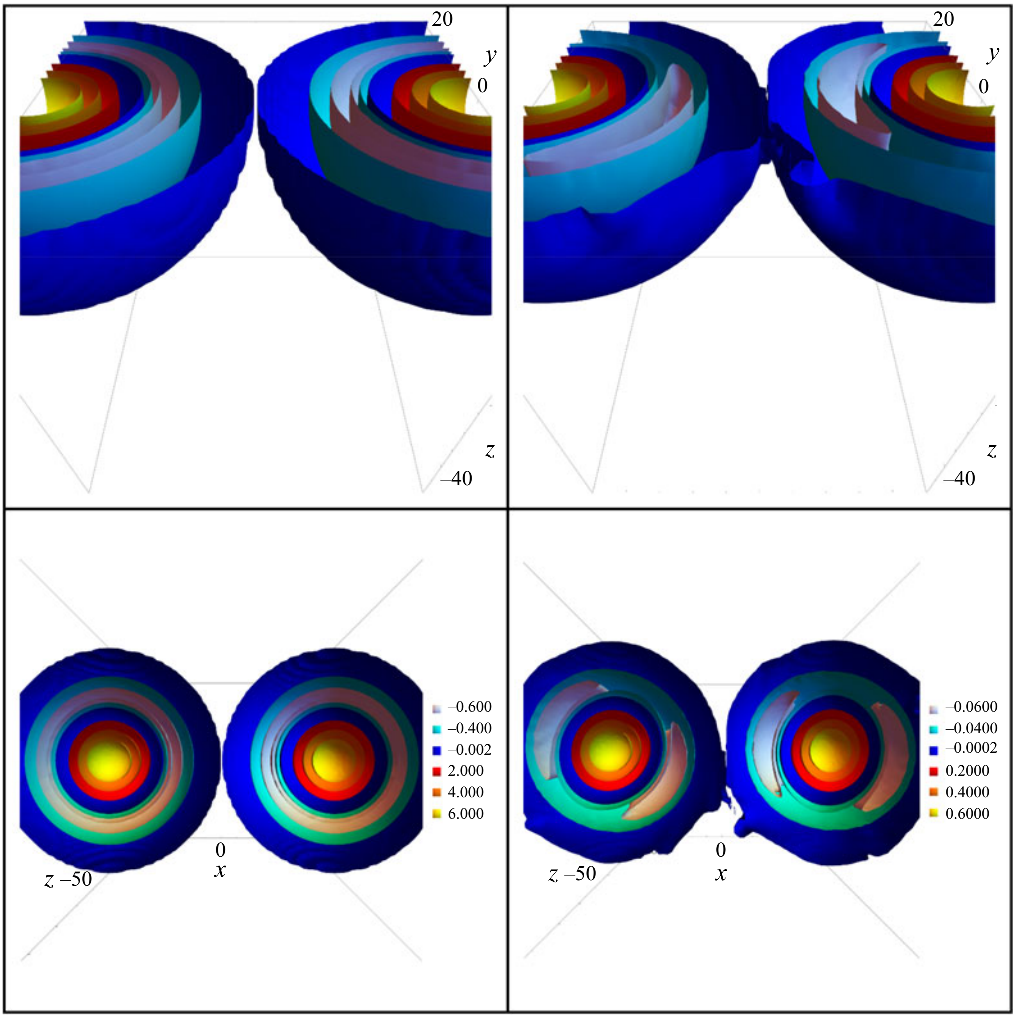

Figure 7. Images of the PVA $\varpi \times 10$ of two initially touching ϖ_u vortices at times (*a*) $t = 0$ and (*b*) $t = 3960$ using the 3-D QG pseudo-spectral code. The top row shows a side view, while the bottom row shows a top view.

strongly interact over a height range comparable to that of the original vortices (Reinaud & Dritschel 2005). Therefore shielding greatly diminishes the vortex interaction, in particular the exchange of material. The exchange generates a small dipolar moment (smaller than in two dimensions), predominantly in layers close to the vortex mid-plane. This causes the vortices to move slightly apart and the azimuthal PVA variations are subsequently redistributed along the vortex peripheries.

Notably, the interaction and PVA exchange between the vortices, in both the contour advection and pseudo-spectral simulations, does not occur when the vortex boundaries are at least one diameter apart from each other. Then, the vortices evolve into compact tripoles, moving apart from each other at late times. When the initial separation distance is reduced to half of a vortex diameter, PVA exchange and subsequent vortex oscillations again occur. Nolan, Montgomery & Grasso (2001) observed that in 3-D baroclinic hurricane-like vortices an asymmetric instability of azimuthal wavenumber $m = 1$ grows which leads to inner-core vorticity redistribution and the displacement of the vortex centre, so that the vortex acquires a small-amplitude trochoidal wobble.

4. Concluding remarks

The present idealised study has focused on the interaction of neutral, shielded vortices in both 2-D and 3-D QG flows. We have found that some pairs of neutral vortices reach an oscillating near-equilibrium state due to a (potential) vorticity exchange mechanism. This oscillating near-equilibrium mechanism is new. It involves a periodic exchange of vorticity and the generation of dipolar moments within the vortices. These dipolar moments separate the vortices. However, the formation of an exterior potential flow arising from the breaking of circular symmetry, and the subsequent vorticity advection and redistribution of peripheral vorticity causes the vortices to attract. Again a dipolar moment grows, and again the vortices move apart, resulting in an oscillating near-equilibrium state between the vortices.

Our results have been verified using independent and markedly different numerical models, namely a pseudo-spectral model and a high-resolution contour-advection model, both in two and three dimensions. The models exhibit a qualitatively similar behaviour, with differences arising predominantly from numerical diffusion. This shows that the solutions given by Viúdez (2021) and Zoeller & Viúdez (2023*b*) are robust. The idealised initial conditions used in this work suggest that the particular vorticity and potential vorticity distributions assumed could provide a plausible explanation for the persistence of some vortices in the ocean, even when they are interacting with other vortices. Furthermore, we have also seen that shielding, occurring when the area or volume integrated vorticity vanishes within each vortex, greatly weakens and retards the interaction. This is particularly evident in 3-D QG flows, since there potential vorticity exchange only occurs near the vortex mid-planes.

The vortex configurations are not all equally robust. In some cases (and in many additional ones not reported in this study), there is a small vorticity leakage from the vortex peripheries to the exterior flow. This vorticity leakage is seen for example in the contour-advection simulation (figure 4). This vorticity transport to the exterior flow is small but can accumulate with time, thereby partially breaking down the shielding effect, which in turn causes the whole configuration to start rotating. The sign of rotation is the same as that of the exterior flow near the vortices. Eventually, this exterior vorticity can become large enough to prevent vorticity exchange and may arrest the oscillations.

We acknowledge that such vortices, which are no longer entirely shielded, may be widespread in geophysical flows. While we do not address their interactions in the present study, our findings for shielded vortices nonetheless help us understand how shielding can increase the robustness and longevity of vortices. For example, the stable equilibrium state found in this study could be an example of what Chouksey, Gula & Carton (2023) identified as a 'doublet' of two same-signed, deep-water coherent vortices, in their study of the coexistence of two anticyclonic vortices over their lifetimes in the North Atlantic. A similar oscillating behaviour to that seen between neutral vortices in the present study (including small vorticity exchange) has been observed for two finite-area, uniform-temperature vortices when separated at a certain distance by Carton *et al.* (2016) in a surface QG model. However, the separation distance between the vortices where the near equilibrium occurs has a much wider range in the present study, from vortices touching at their boundaries to vortices being separated between their boundaries by $\delta_0 = j_{3/2,2}/2 = 3.86$. Additionally, none of the interactions investigated here led to merging, because of shielding, even when the vortices at the beginning were touching.

In future research, it would be worth carrying out a weakly nonlinear stability analysis on these 3-D QG vortices to better understand the formation of vortex tripoles. Furthermore, one could investigate similar vorticity exchange interactions but extended to a set of multiple (more than 2) vortices similar to the ones described in Viúdez (2021). Groups of two or more coherent vortices travelling together have been observed in the oceans in deep water (Chouksey 2023). Additionally, other parameter variations should be examined, such as shielded vortices but of opposite sign, or two vortices of different sizes, or offset vertically in the 3-D QG model.

Acknowledgements. We are very grateful to three anonymous reviewers for their very helpful comments on this manuscript. We also acknowledge the 'Severo Ochoa Centre of Excellence' accreditation (CEX2019-000928-S).

Funding. This work has been funded by the Spanish Government through the project SAGA (Ministerio de Ciencia, Innovacion y Universidades, Ref. No. RTI2018-100844-B-C33) and the FPI PhD grant given to V.Z. (Ministerio de Ciencia e Innovacion PRE2019-090309). Furthermore, the exchange between the ICM and St Andrews University was facilitated by the Erasmus+ Programme of the European Union through a short-term doctoral mobility grant.

Declaration of interests. The authors report no conflicts of interest.

Appendix A. Pseudo-spectral numerical model

The numerical simulations have been carried out using a 2-D and a 3-D pseudo-spectral code in doubly and triply periodic domains, respectively, using a leap-frog time-stepping method together with a weak Robert–Asselin time filter to avoid the decoupling of even and odd time levels. This follows the approach of Dritschel & Viúdez (2003), where the equation of material conservation of vorticity (2.7) or QG PVA (2.1) is numerically integrated in time, as detailed in Zoeller & Viúdez (2023*a*). The numerical hyperviscosity e-folding rate e_f was chosen as small as possible ($e_f = 0.2$ in 3-D QG and $e_f = 1$ in two dimensions) to prevent the growth of numerical noise.

In the 2-D case, the spatial domain uses a numerical grid of $n_x \times n_y = 1024 \times 1024$ grid points, and the horizontal extent is $L_x = L_y = 40$. In the 3-D QG case, the number of grid points is $n_x \times n_y \times n_z = 256^3$, which is relatively coarse in order to enable the analysis of a large number of long numerical simulations. The time step is fixed at $\delta t = 0.01$ as there is no growth of vorticity or PVA – the flow does not speed up. The horizontal and (stretched) vertical extent is $L_x = L_y = c_0 L_z = 40$ (where $c_0 = N_0/f_0$), which is large compared with the radii of the vortices, $r_p = j_{1,p}$ with $\{j_{1,2}, j_{1,3}\} \simeq \{7.01, 10.17\}$ in the 2-D case and $\{j_{3/2,2}, j_{3/2,3}\} \simeq \{7.73, 10.9\}$ in the 3-D case. The 3-D numerical results are independent of the ratio $c_0 \equiv N_0/f_0$. Typical geophysical (atmospheric and oceanographic) applications of the 3-D QG model assume values $c_0 \in [10, 100]$.

Appendix B. Contour-advection numerical model

In contour advection, the vorticity field in two dimensions, or the PVA field on each isopycnal surface in three dimensions, is discretised into a finite set of contours, each of which consists of a variable number of nodes connected together by local cubic splines. Across each contour, the vorticity or PVA jumps by a fixed, prescribed amount, equal to $(\zeta_{max} - \zeta_{min})/n_l$ or $(\varpi_{max} - \varpi_{min})/n_l$, with $n_l = 100$ (a large value which well represents the actual continuous distributions).

The 2-D model uses the CLAM developed by Dritschel & Fontane (2010), which is an extension of the contour-advective semi-Lagrangian (CASL) algorithm developed by

Dritschel & Ambaum (1997). The CLAM combines a pseudo-spectral method, which is especially accurate for large scales and energy conservation, with Lagrangian contours, which accurately and efficiently represent intermediate to small scales, well below those available to the pseudo-spectral method. The CLAM allows for the representation of general forcing and dissipation (non-conservation), although this feature is not used here. The basic (inversion) grid resolution is 1024^2, but studies show that the effective grid resolution is approximately 16 times higher in each dimension (Dritschel & Tobias 2012). The range of the spatial numerical domain is $[-\pi, \pi] \times [-\pi, \pi]$.

The 3-D QG model extends the 2-D CASL model (Dritschel & Ambaum 1997), to permit one to study the dynamics of complex, fine-scale conservative potential vorticity distributions in three dimensions (Dritschel, de la Torre Juárez & Ambaum 1999). The basic (inversion) grid resolution is 256^3, although the effective resolution is much higher. In the vertical, 4 times as many isopycnal surfaces are used than grid points to better represent the vertical variation of the potential vorticity field. We fix the extent of the (triply periodic) physical domain to be $(2\pi)^3$ and rescale the radii of the vortices and the distances between them to ensure that all vortex configurations have identical total circulation and are not strongly affected by the flow periodicity. The method is essentially inviscid, with 'contour surgery' being the only source of pseudo-diffusion (Dritschel 1988). The initial conditions are unperturbed.

Appendix C. Linear stability of a two-dimensional shielded vortex

We analyse the linear stability of a single 2-D shielded vortex. The vorticity field ζ is discretised using N equal jumps $\Delta q = (\zeta_{max} - \zeta_{min})/N$ spanning the range of vorticity $(\zeta_{min}, \zeta_{max})$ within the vortex. We then discretise the vortex by $N_c > N$ circular contours $\mathcal{C}_j$ of radii $\bar{\rho}_j$, for $1 \le j \le N_c$. The radii are determined from $\zeta(\bar{\rho}_j) = \zeta_{min} + (i - 0.5)\Delta q$, for $1 \le i \le N$ (N_c exceeds N because ζ is non-monotonic in a shielded vortex). We associate the signed vorticity jump $\Delta q_j = \pm\Delta q$ with the contour $\mathcal{C}_j$ depending on whether the vorticity increases or decreases across the contour in the direction of decreasing radius.

To examine linear stability, we displace each contour radially

$$\rho_i(\varphi, t) = \bar{\rho}_i + \epsilon\eta_i e^{i(m\varphi - \sigma t)}, \tag{C1}$$

where $\epsilon \ll 1$, $\epsilon\eta_i$ is the complex amplitude (the real part of ρ_i is intended), and $\sigma(m) = \sigma_r(m) + i\sigma_i(m)$ is the eigenvalue to be determined (σ_r gives the growth rate while σ_i gives the frequency of wave-like disturbances). The circular symmetry of the basic-state flow permits us to study each azimuthal wavenumber $m = 1,\ 2\ \ldots$ separately.

The kinematic condition on contour $\mathcal{C}_i$ is

$$\frac{\mathrm{D}\rho_i}{\mathrm{D}t} = i(m\bar{\Omega}_i - \sigma)\eta_i = v_i, \tag{C2}$$

where $\bar{\Omega}_i = \bar{u}_i/\rho_i$ is the basic-state angular velocity, while v_i is the radial velocity. The latter is obtained by contour integration over the N_c contours

$$v_i(\varphi, t) = \sum_{j=1}^{N_c} \Delta q_j \oint_{\mathcal{C}_j} G(\rho_i(\varphi, t), \rho_j(\varphi', t))\mathrm{d}\varphi', \tag{C3}$$

where G is the Green's function giving the contribution of contour $\mathcal{C}_j$ to contour $\mathcal{C}_i$. Linearising (C3) for $\epsilon \ll 1$ leads to

$$(m\bar{\Omega}_i - \sigma)\eta_i = \sum_{i=1}^{N_c} \Delta q_j \mathcal{K}(\bar{\rho}_i, \bar{\rho}_j)\eta_j, \tag{C4}$$

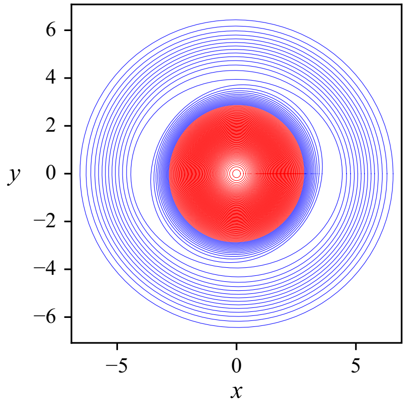

Figure 8. Contours (vorticity jumps) C_j, $1 \leq j \leq N_c$, deformed by the unstable eigenmode with azimuthal number $m = 2$, using $N = 100$, for the ζ_u vortex. The red contours correspond to the region where $\zeta > 0$, while the blue contours correspond to the region where $\zeta < 0$.

where

$$\mathcal{K}(\bar{\rho}_i, \bar{\rho}_j) = \frac{1}{2} \begin{cases} \left(\dfrac{\bar{\rho}_i}{\bar{\rho}_j}\right)^{1+m}, & \text{for} \quad \bar{\rho}_i < \bar{\rho}_j, \\ \left(\dfrac{\bar{\rho}_i}{\bar{\rho}_j}\right)^{1-m}, & \text{for} \quad \bar{\rho}_i \geq \bar{\rho}_j, \end{cases} \tag{C5}$$

see Flierl (1988). For each m, this results in an $N_c \times N_c$ eigenvalue problem for σ and the associated eigenvector η_j $(1 \leq j \leq N_c)$. In general, there are N_c eigenvalues σ.

For the ζ_u vortex, only azimuthal mode $m = 2$ is linearly unstable, with a growth rate $\sigma_i = 0.042$ and $\sigma_r = 0.25$ (to two digits of accuracy). Convergence of the results has been tested by varying the number of vorticity jumps N from 100 to 5000. Figure 8 shows the contour deformation of the eigenmode for $N = 100$. The greatest deformation occurs near the centre of the vorticity profile, in the region of weak negative vorticity. By contrast, the ζ_s vortex has been found to be linearly stable for all m.

References

Barabinot, Y., Reinaud, J.N., Carton, X.J., de Marez, C. & Meunier, T. 2024 A 3-D minimum-enstrophy vortex in stratified quasi-geostrophic flows. *J. Fluid Mech.* **986**, R1.

Beckers, M., Verzicco, R., Clercx, H.J.H. & van Heijst, G.J.F. 2001 Dynamics of pancake-like vortices in a stratified fluid: experiments, model and numerical simulations. *J. Fluid Mech.* **433**, 1–27.

Brown, G.L. & Roshko, A. 1974 On density effects and large structure in turbulent mixing layers. *J. Fluid Mech.* **64** (4), 775–816.

Carton, X. 2001 Hydrodynamical modeling of oceanic vortices. *Surv. Geophys.* **22**, 179–263.

Carton, X., Ciani, D., Verron, J., Reinaud, J. & Sokolovskiy, M. 2016 Vortex merger in surface quasi-geostrophy. *Geophys. Astrophys. Fluid Dyn.* **110**, 1–22.

Carton, X., Daniault, N., Alves, J., Cherubin, L. & Ambar, I. 2010 Meddy dynamics and interaction with neighboring eddies southwest of Portugal: observations and modeling. *J. Geophys. Res.: Oceans* **115** (C6), C06017.

Carton, X. & Legras, B. 1994 The life-cycle of tripoles in two-dimensional incompressible flows. *J. Fluid Mech.* **267**, 53–82.

Carton, X.J. 1992 On the merger of shielded vortices. *Europhys. Lett.* **18** (8), 697.

Chan, J.C.L. & Law, A.C.K. 1995 The interaction of binary vortices in a barotropic model. *Meteorol. Atmos. Phys.* **56**, 135–155.

Chouksey, A. 2023 Long-lived deep coherent vortices in the Atlantic ocean. PhD thesis, Université de Bretagne Occidentale.

Chouksey, A., Gula, J. & Carton, X.J. 2023 *Long-Lived Deep Coherent Vortices in the Northeast Atlantic Ocean*. ESS Open Archive.

Christiansen, J.P. & Zabusky, N.J. 1973 Instability, coalescence and fission of finite-area vortex structures. *J. Fluid Mech.* **61** (2), 219–243.

Ciani, D., Carton, X. & Verron, J. 2016 On the merger of subsurface isolated vortices. *Geophys. Astrophys. Fluid Dyn.* **110** (1), 23–49.

Dritschel, D.G. 1985 The stability and energetics of corotating uniform vortices. *J. Fluid Mech.* **157**, 95–134.

Dritschel, D.G. 1988 Contour surgery: a topological reconnection scheme for extended integrations using contour dynamics. *J. Comput. Phys.* **77**, 240–266.

Dritschel, D.G. 1995 A general theory for two-dimensional vortex interactions. *J. Fluid Mech.* **293**, 269–303.

Dritschel, D.G. & Ambaum, M.H.P. 1997 A contour-advective semi-lagrangian numerical algorithm for simulating fine-scale conservative dynamical fields. *Q. J. R. Meteorol. Soc.* **123** (540), 1097–1130.

Dritschel, D.G. & Fontane, J. 2010 The combined Lagrangian advection method. *J. Comput. Phys.* **229** (14), 5408–5417.

Dritschel, D.G. & Tobias, S.M. 2012 Two-dimensional magnetohydrodynamic turbulence in the small Prandtl number limit. *J. Fluid Mech.* **703**, 85–98.

Dritschel, D.G., de la Torre Juárez, M. & Ambaum, M.H.P. 1999 The three-dimensional vortical nature of atmospheric and oceanic turbulent flows. *Phys. Fluids* **11** (6), 1512–1520.

Dritschel, D.G. & Viúdez, A. 2003 A balanced approach to modelling rotating stably stratified geophysical flows. *J. Fluid Mech.* **488**, 123–150.

Dritschel, D.G. & Waugh, D.W. 1992 Quantification of the inelastic interaction of unequal vortices in two-dimensional vortex dynamics. *Phys. Fluids* **4**, 1737–1744.

Flierl, G.R. 1988 On the instability of geostrophic vortices. *J. Fluid Mech.* **197**, 349–388.

Holland, G.J. & Dietachmayer, G.S. 1993 On the interaction of tropical-cyclone-scale vortices. iii: continuous barotropic vortices. *Q. J. R. Meteorol. Soc.* **119** (514), 1381–1398.

Kizner, Z. & Khvoles, R. 2004 The tripole vortex: experimental evidence and explicit solutions. *Phys. Rev. E Statist. Nonlinear Soft Matt. Phys.* **70** (1), 016307.

Melander, M.V., Zabusky, N.J. & McWilliams, J.C. 1988 Symmetric vortex merger in two dimensions: causes and conditions. *J. Fluid Mech.* **195**, 303–340.

Morel, Y. & Carton, X. 1994 Multipolar vortices in two-dimensional incompressible flows. *J. Fluid Mech.* **267**, 23–51.

Nolan, D.S., Montgomery, M.T. & Grasso, L.D. 2001 The wavenumber-one instability and trochoidal motion of hurricane-like vortices. *J. Atmos. Sci.* **58** (21), 3243–3270.

Paireau, O., Tabeling, P. & Legras, B. 1997 A vortex subjected to a shear: an experimental study. *J. Fluid Mech.* **351**, 1–16.

Perrot, X. & Carton, X. 2010 2-D vortex interaction in a non-uniform flow. *Theor. Comput. Fluid Dyn.* **24**, 95–100.

Reinaud, J.N. & Dritschel, D.G. 2005 The critical merger distance between two co-rotating quasi-geostrophic vortices. *J. Fluid Mech.* **522**, 357–381.

Ritchie, E.A. & Holland, g J. 1993 On the interaction of tropical-cyclone-scale vortices. ii: discrete vortex patches. *Q. J. R. Meteorol. Soc.* **119** (514), 1363–1379.

Rodríguez-Marroyo, R., Viúdez, A. & Ruiz, S. 2011 Vortex merger in oceanic tripoles. *J. Phys. Oceanogr.* **41** (6), 1239–1251.

Schmidt, M.R., Beckers, M., Nielsen, A.H., Rasmussen, J.Juul & van Heijst, G.J.F. 1998 On the interaction between two oppositely signed, shielded, monopolar vortices. *Phys. Fluids* **10** (12), 3099–3110.

Schultz Tokos, K.L., Hinrichsen, H.-H. & Zenk, W. 1994 Merging and migration of two meddies. *J. Phys. Oceanogr.* **24** (10), 2129–2141.

Trieling, R., van Heijst, G. & Kizner, Z. 2010 Laboratory experiments on multipolar vortices in a rotating fluid. *Phys. Fluids* **22**, 094104.

Valcke, S. & Verron, J. 1997 Interactions of baroclinic isolated vortices: the dominant effect of shielding. *J. Phys. Oceanogr.* **27** (4), 524–541.

Viúdez, A. 2021 Robust and unstable axisymmetric vortices, including neutral vortices, of a new two-dimensional vortex family. *Phys. Fluids* **33** (5), 054103.

Wang, Y. & Holland, G.J. 1995 On the interaction of tropical-cyclone-scale vortices. iv: baroclinic vortices. *Q. J. R. Meteorol. Soc.* **121** (521), 95–126.

Waugh, D.W. 1992 The efficiency of symmetric vortex merger. *Phys. Fluids A: Fluid Dyn.* **4** (8), 1745–1758.

WINANT, C.D. & BROWAND, F.K. 1974 Vortex pairing: the mechanism of turbulent mixing-layer growth at moderate reynolds number. *J. Fluid Mech.* **63** (2), 237–255.

YASUDA, I., OKUDA, K. & HIRAI, M. 1992 Evolution of a Kuroshio warm-core ring–variability of the hydrographic structure. Deep sea research part A. *Oceanogr. Res. Papers* **39**, S131–S161.

ZOELLER, V. & VIÚDEZ, A. 2023*a* Elastic interaction between a mesoscale eddy-pair and an axisymmetrical eddy. *J. Geophys. Res.: Oceans* **128** (3), e2022JC019597.

ZOELLER, V. & VIÚDEZ, A. 2023*b* Three-dimensional quasi-geostrophic vortices with vanishing amount of potential vorticity anomaly. *Phys. Fluids* **35** (12), 126607.

ZOELLER, V. & VIÚDEZ, A. 2024 Two-dimensional shielded vortices in a shear current. *Phys. Fluids* **36** (5), 056602.